SLAC-PUB-1257
(T/E)
June 1973

THE ANALYSIS OF $\pi N \rightarrow \pi\pi N$ AND COUPLED CHANNEL ANALYSES OF πN REACTIONS*

Roger J. Cashmore

Stanford Linear Accelerator Center

Stanford University, Stanford, California 94305

ABSTRACT

The status of partial wave analyses of $\pi N \rightarrow \pi\pi N$ in the energy range $1300 < E < 2000$ MeV is reviewed. In the majority of partial waves the total πN inelasticity is accounted for and the inelastic decay channels of many resonances are observed. In total 23 resonance couplings to the states $\pi\Delta$, $N\rho$, $N\epsilon$ are measured both in magnitude and sign. The D_{13} state in the region of 1700 MeV is unambiguously observed while there is a conspicuous absence of P_{33} states below 2000 MeV. Coupled channel analyses of these partial wave amplitudes, exploiting unitarity to the fullest extent, have been performed resulting in pole positions and residues for all resonant states with mass < 1900 MeV. Finally the different methods of estimating resonance parameters are discussed and the results contrasted.

I. INTRODUCTION

Most of our present information on the resonance region in πN reactions has been derived from the extensive phase shift analyses of differential cross sections and polarization data[1,2] in elastic scattering and charge exchange reactions

$$\pi^{\pm} p \rightarrow \pi^{\pm} p \tag{1}$$

$$\pi^{-} p \rightarrow \pi^{o} n \tag{2}$$

*Work supported by the U. S. Atomic Energy Commission.

(Presented at the Purdue Conference on Baryon Resonances, West Lafayette, Indiana, April 20-21, 1973.)

To complete our knowledge for $E_{c.m.} < 2000$ MeV we need to study the inelastic reactions which constitute as much as 50% of the total cross section at these energies. This implies detail study of the single pion production reactions

$$\pi^- p \to \pi^+ \pi^- n, \quad \pi^- \pi^o p, \quad \pi^o \pi^o n \tag{3}$$

$$\pi^+ p \to \pi^+ \pi^o p, \quad \pi^+ \pi^+ n \tag{4}$$

At $E_{c.m.} = 1520$ MeV $\sim$13 mb of the total inelastic $\pi^- p$ cross section of 15 mb is accounted for by reactions (3) while at $E_{c.m.} = 1700$ MeV the numbers are respectively $\sim$21-22 mb out of $\sim$25 mb.

Thus we conclude that if the $\pi\pi N$ final states can be understood we will have an essentially complete description of πN scattering at these energies. We will then be in a position to attempt a multichannel analysis of the πN reactions with the added knowledge that no further new experimental information will become available (although, of course, the present inelastic partial wave amplitudes may be somewhat modified in light of new results, e.g., polarization measurements in the inelastic reactions).

In this talk I will attempt to review two topics

(1) the present status of partial wave analyses (PWA) of $\pi N \to \pi\pi N$

(2) the status of multichannel fits to all of the πN reactions.

II. THE PARTIAL WAVE ANALYSES OF $\pi N \to \pi\pi N$

In general two methods have been followed: isobar model analyses of the whole final state,[3,4] and the analysis of specific reactions, e.g., $\pi N \to \pi\Delta$ (Ref. 5) which have been isolated by applying judicious cuts to the data to select this final state.

A. Isobar Model Analysis

Groups in Oxford,[6,7] Saclay[8] and LBL/SLAC[9] have used this technique differing mainly in their methods of fitting the data. The method itself consists of writing the transition amplitude for reaching a given $\pi\pi N$ final state as a coherent sum of quasi two-body processes as indicated in Fig. 1. The transition matrix is then written in an LS representation as[3,4]

$$T(W, w_1, w_2, \theta, \phi) = \sum_{JLSI} A^{IJLS\ell} \times C^I X^{JLS\ell}(w_1, w_2, \theta, \phi)\, B^\ell(w_1, w_2) \tag{5}$$

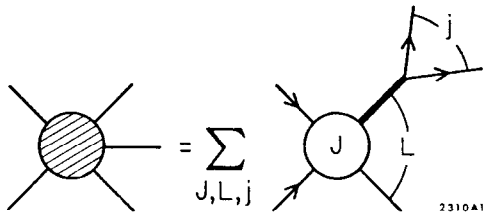

FIG. 1--The isobar model.

where: $w, w_1, w_2, \theta, \phi$ are the kinematic variables required to completely specify the reaction; C^I is the product of isospin Clebsch-Gordon coefficients to reach different charge final states; $X^{JLS\ell}$ contains all factors related to the angular momentum decompositions, including barrier factors; $B^{\ell}(w_1, w_2)$ is the final state enhancement factor, e.g., a Breit-Wigner or Watson Final State Interaction factor,[10] where ℓ is the orbital angular momentum in the decay of the isobar. The variable parameters, the partial wave amplitudes, $A^{IJLS\ell}$ are assumed to be dependent only on the total c.m. energy W. The differential cross section is

$$d^4\sigma(w, w_1, w_2, \theta, \phi) \propto |T(w, w_1, w_2, \theta, \phi)|^2 \tag{6}$$

The data is fitted in a variety of manners by the different groups, always treating each c.m. energy independently — Oxford[6,7] fit invariant mass and angular projections of the data in $\pi^{\pm}p$ collisions for $1300 < E < 1500$; Saclay[8] fit moments of the angular distribution as a function of mass for π^-p in the range $1390 < E < 1580$ and π^+p in the range $1650 < E < 1970$; LBL/SLAC[9] make maximum likelihood fits to $\pi^{\pm}p$ reactions for $1300 < E < 1970$ (ie., to all the variables).

This isobar model approach is optimistic in that one hopes to fit the whole reaction making maximum use of all interference effects associated with the overlap of the various resonance bands. However, as we shall see this has proved to be possible and provides us with an immense amount of information.

B. Partial Wave Analysis of Specific Reaction

The SLAC/LBL[11] collaboration and an LBL/UC Riverside[12] group have used this technique to analyze specifically

$$\pi N \rightarrow \pi\Delta \tag{7}$$

After applying cuts, one assumes that one has a pure sample of reactions (7) and then performs fits to the production angular distribution of the Δ and sometimes also its density matrix elements, in terms of the partial wave amplitudes, usually with an energy dependent formalism. The major advantage in this case is that the formalism is easier to handle whereas the great dangers lie in the assumption of a pure sample and the energy dependent parameterizations one uses. Furthermore, it is impossible to relate in phase, reactions such as

$$\pi N \rightarrow N\rho \tag{8}$$

to reactions (7) because the regions of interference which would define the phase are specifically removed from consideration. I feel that this method provides useful information but only on the large unambiguous partial waves present, and one should be much more skeptical of small effects.[11]

III. THE SLAC/LBL PARTIAL WAVE ANALYSIS OF $\pi N \rightarrow \pi\pi N$

In order to make a coherent review I am going to concentrate on our analysis at SLAC and LBL for the following reasons:

(i) It spans the c.m. energy range $1300 < E < 2000$ except for a 100 MeV gap $1540 < E < 1650$ where the data is not yet available to us.

(ii) It utilizes the data in the most efficient manner making a simultaneous maximum likelihood fit[9, 13] to the three major channels at each energy

$$\begin{aligned} \pi^- p &\rightarrow \pi^+ \pi^- n \\ \pi^- p &\rightarrow \pi^- \pi^o p \\ \pi^+ p &\rightarrow \pi^+ \pi^o p \end{aligned} \qquad (9)$$

(iii) We obtain excellent agreement with the inelastic reaction cross sections predicted by elastic phase shift analyses (EPSA).

(iv) We have been able to identify a continuous solution throughout our energy range from the independent solutions at each energy, thus allowing us to show reliable Argand diagrams for the first time.

I will then use the results of the other groups to substantiate our results and where necessary note differences.

The isobar final states that we have specifically considered are

$\pi N \rightarrow \pi\Delta$

$\rightarrow N\rho$ S(the total intrinsic $N\rho$ spin) $= \frac{1}{2}$ or $\frac{3}{2}$ referred to as ρ_1 or ρ_3

$\rightarrow N\epsilon$

The results are then presented as partial wave amplitudes in an LS representation of the T-matrix after having made maximum likelihood fits to the data at the 18 energies we have considered. These energies and the data used are noted in Table I where the lack of data from 1540 to 1650 should be noted.

In order to emphasize these results I have to demonstrate their quality. Table II represents the χ^2 at 3 energies in our analysis, the ratio χ^2/N being excellent at lower energies but deteriorating as the energy increases. There are enormous variations of structure within the data at a given energy and in general the model reproduces these well, as can be seen in Fig. 2 which shows our 4-D representation of the fit to $\pi^+\pi^-n$ at 1690 MeV.

TABLE I

Number of events for the energy bins used in the fits.

C.M. Energy	Range (MeV)	$\pi^- p \rightarrow \pi^+ \pi^- n$	$\pi^- p \rightarrow \pi^- \pi^o p$	$\pi^+ p \rightarrow \pi^+ \pi^o p$
1310	1300-1330	1069	151	
1340	1330-1360	1664	11	
1370	1360-1380	2471	2	
1400	1380-1410	5049	964	78
1440	1430-1460	4918	1802	359
1470	1460-1480	3252	1629	175
1490	1480-1510	5555	3197	1523
1520	1510-1530	3241	2588	795
1540	1530-1560	3905	3285	1114
1650	1630-1670	6061	3757	2467
1690	1670-1710	5901	3689	1139
1730	1710-1750	3455	2630	4061
1770	1750-1790	3214	2352	2853
1810	1790-1830	2447	1541	3855
1850	1380-1870	3931	3183	6372
1890	1870-1910	5072	3170	12690
1930	1910-1950	5817	4080	4298
1970	1950-1990	5277	3544	7744
Total	1300-1990	72299	41575	49523

TABLE II

Summary of χ^2 at specimen energies. The predicted bin populations are derived from maximum likelihood fits to the data.

$E_{c.m.}$	χ^2	N_{bins}	Number of Partial Waves
1530	790	681	15
1690	1086	679	20
1970	2372	702	24

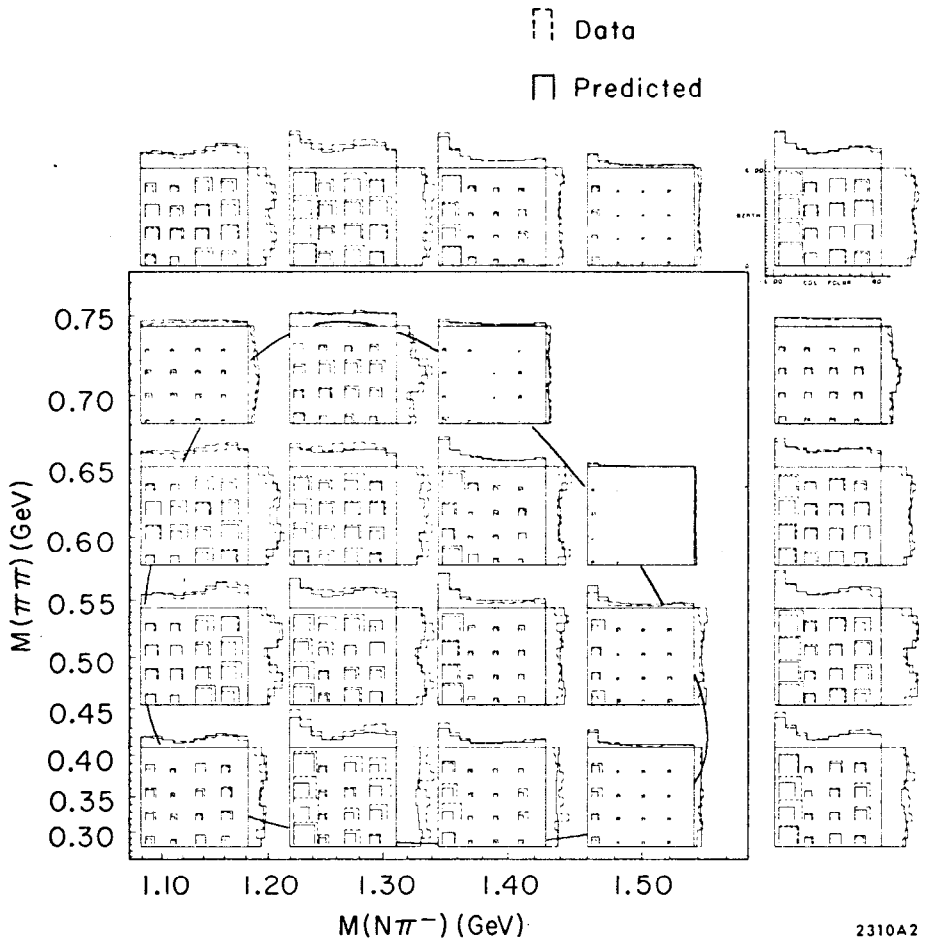

FIG. 2--Fits to the reaction $\pi^- p \rightarrow \pi^+ \pi^- n$ at a c.m. energy of 1690 MeV. The figure contains cos θ vs ϕ plots for individual regions of the Dalitz plot where cos θ and ϕ are the polar angles of the incident pion in a coordinate system defined by the final state. The z axis lies along $\vec{p}_N$ and the y axis lies along $\vec{p}_{\pi^-} \times \vec{p}_{\pi^+}$. The plots outside the Dalitz plot are the sums of the corresponding plots within the boundary.

This figure consists of 2-D plots of the angular variables, cos θ and ϕ, for individual regions of the Dalitz plot. We can also use our partial wave amplitudes to predict the cross section for

$$\pi^- p \rightarrow \pi^0 \pi^0 n \tag{10}$$

and the good agreement with the experimental results is demonstrated in Fig. 3. Finally, and this will be continually apparent throughout this talk, we have excellent agreement with EPSA predictions.

The remaining point that must be addressed is the question of uniqueness of the solutions. For energies below 1540 MeV we are fairly certain of a unique solution because many random starting values always lead to one final solution. For energies greater than 1650 MeV we cannot be certain. We obtain several solutions at each energy from which we have identified the present solution by requiring reasonable agreement with EPSA predictions and continuity to the solution at the adjacent energy points. These points of continuity in modulus and phase are vitally important because this allows us to show Argand diagrams.

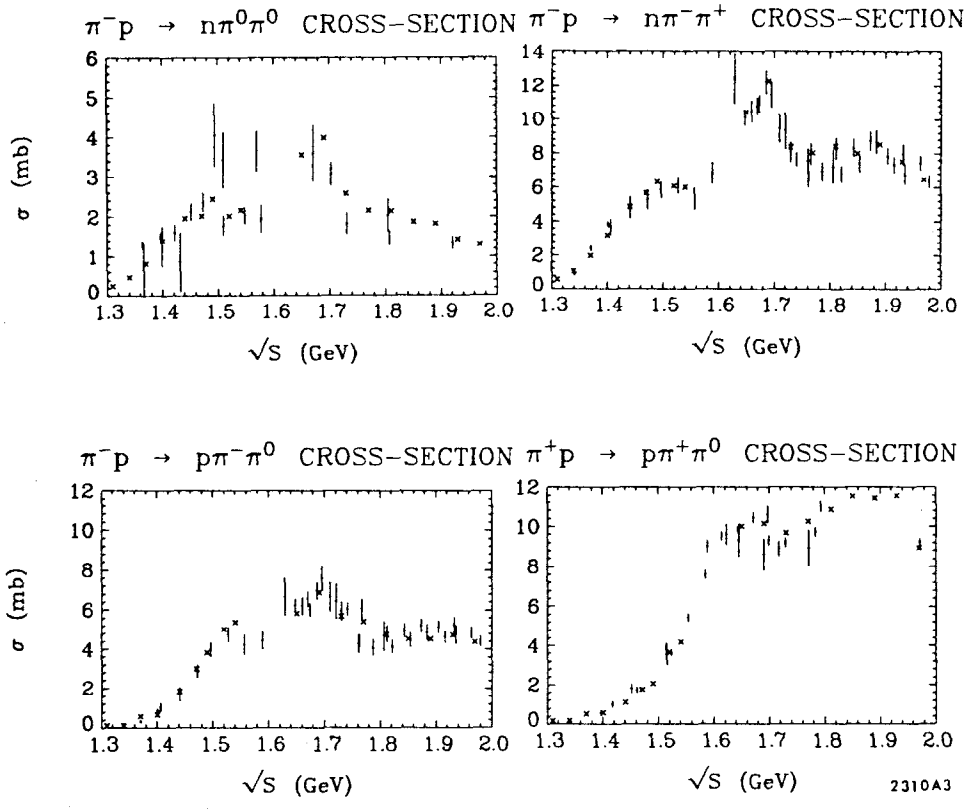

FIG. 3--Single pion production cross sections. Data points are indicated by | and the predictions from our partial wave amplitudes by x.

IV. RESULTS OF PARTIAL WAVE ANALYSES OF $\pi N \rightarrow \pi\pi N$

In analyzing inelastic reactions at a given energy E the relative phases of the individual waves are only determined and not the absolute phase (a distinct difference from elastic phase shift analysis). In order to present Argand diagrams we have to specify the absolute phase at each energy. We have chosen to do this by K-matrix fits to the P11, D15 and F15, F35 partial waves in the low, middle and high regions of our data respectively, sufficient overlap existing so that reliable continuity is obtained. However, we are hampered by the lack of data for $1540 < E < 1650$ in relating the lower energy results to the others. Although we believe we have the correct continuation within our present interpretation, a completely new hypothesis (e.g., a second P11 resonance at ~1540 MeV) could produce changes in this continuation.

A. I=1/2 States

In Fig. 4 I display the Argand diagrams of all of the I=1/2 waves we have determined in our analysis. These figures contain a great deal of information and I will only attempt to point out the most important and striking features.

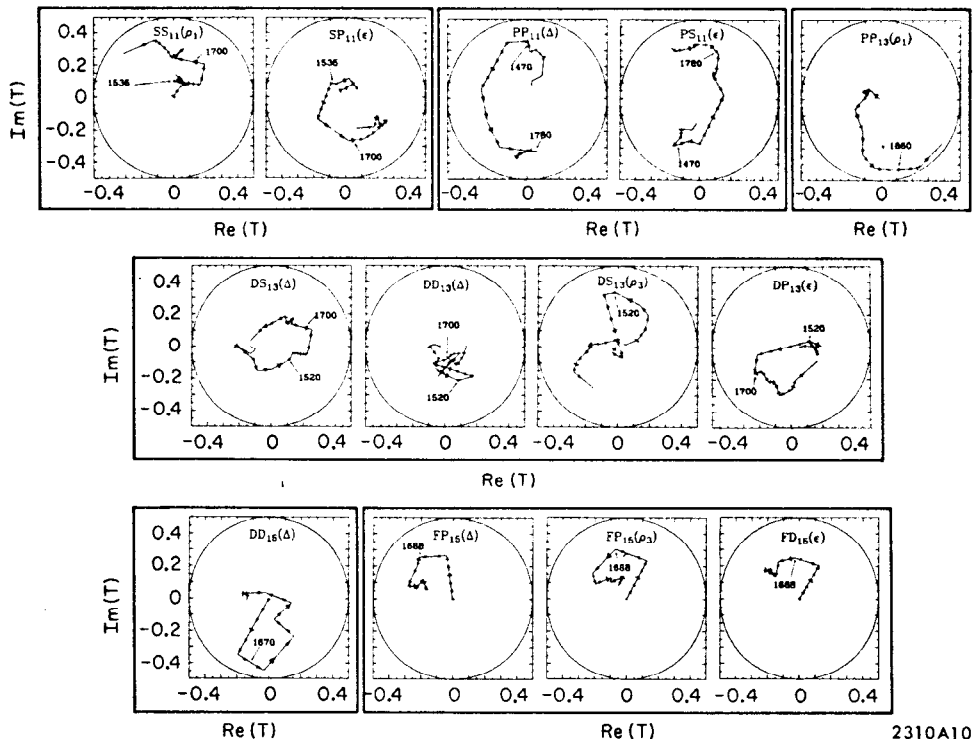

FIG. 4--I=1/2 partial wave amplitudes. Arrows are spaced every 20 MeV, with wide arrows every 100 MeV: base of wide arrows mark integral hundreds of MeV. Lower-ℓ waves are plotted starting at s=1400 MeV; higher-ℓ waves only where they were first needed. Last arrowhead is always at 1940 MeV.

1. The considerable amount of motion of the partial wave amplitudes in these plots is not surprising, essentially all of the structure being associated with the existence of known resonance states.

2. S11. Figure 5 indicates there is little evidence of the N*(1535) in the LBL/SLAC analysis which can be compared with the results presented to

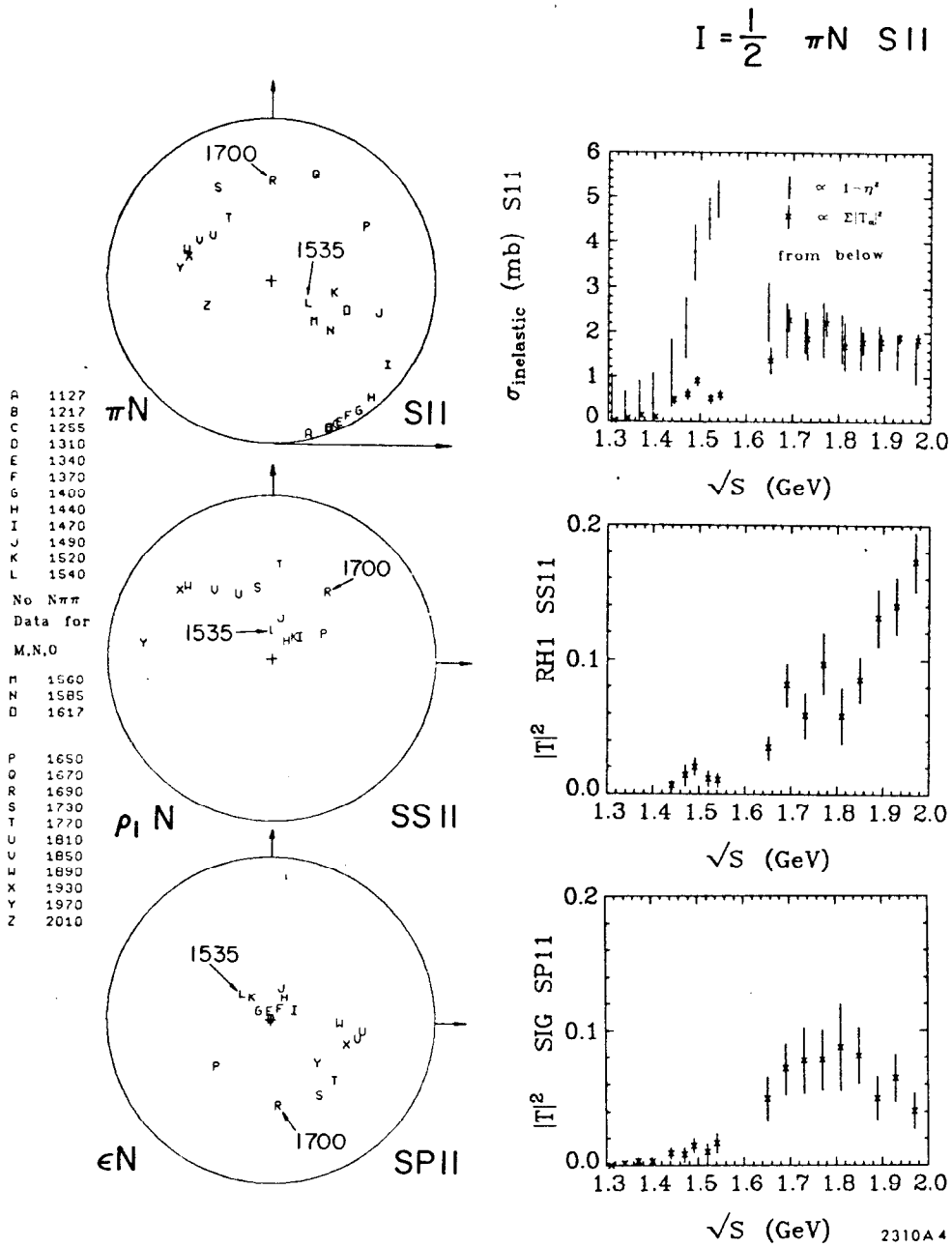

FIG. 5--Partial waves derived from the incident S11 wave.

this conference from the Saclay group[8] in Fig. 6. If the missing cross section in the two cases is ascribed to the ηN channel the two results would imply different branching ratios of the N*(1535) into ηN

SLAC/LBL: $\chi_{\eta N} = 0.55$

— the usually accepted number[14]

Saclay: $\chi_{\eta N} = 0.35$.

Although the result from Saclay is consistent with a recent analysis[15] of

$$\pi^- p \rightarrow \eta n \ , \qquad (11)$$

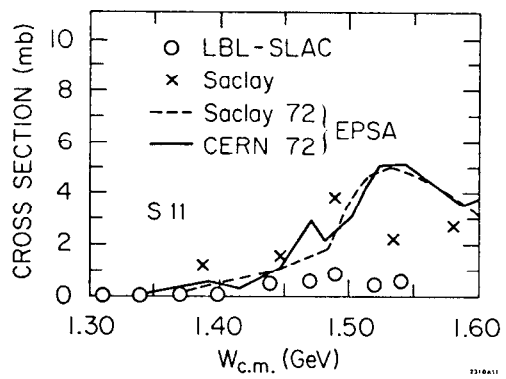

FIG. 6--Comparison of SLAC/LBL and Saclay results for the S11 inelasticity.

there are at least two dubious points in the Saclay analysis:

(i) the phases of the partial wave amplitudes are not continuous[16]

(ii) the comparison with the mass spectra, Fig. 7, are very poor.

Thus there is a disagreement which I think will only be resolved by future analysis.

3. P11. The N*(1470) and N*(1780) resonances are very clear (see Fig. 4), their decays into $\pi\Delta$ and $N\epsilon$ both being strong.

4. $N\rho$ couplings. We observe strong $N\rho$ couplings of the $P_{13}(1860)$, $D_{13}(1520)$ and $F_{15}(1690)$ resonances. This is not really surprising, as the last two resonances are strongly seen in photoproduction and application of VDM would imply this result. Indeed the couplings are of the correct order of magnitude.

5. $D_{13}(1700)$. This state which has been hinted at in EPSA is definitely present in our analysis (see also Fig. 8) decaying strongly into $\pi\Delta$ (DS13) and $N\epsilon$ (DP13) with a total width in the range 100 - 200 MeV. This state has long been required to complete the N* and Δ members of the $(70, 1^-)$ supermultiplet of negative parity baryon states.[17]

6. D15 and F15. These two resonances are strongly observed in this analysis, the result being consistent with solution A, one of two solutions in an earlier analysis of $\pi N \rightarrow \pi\Delta$ which are shown in Fig. 9.[11] Indeed we have never been able to obtain any solution in which these two states have a net positive relative coupling to the $\pi\Delta$ channel.

B. I=3/2 States

In Fig. 10 I show the I=3/2 partial waves that we have determined.

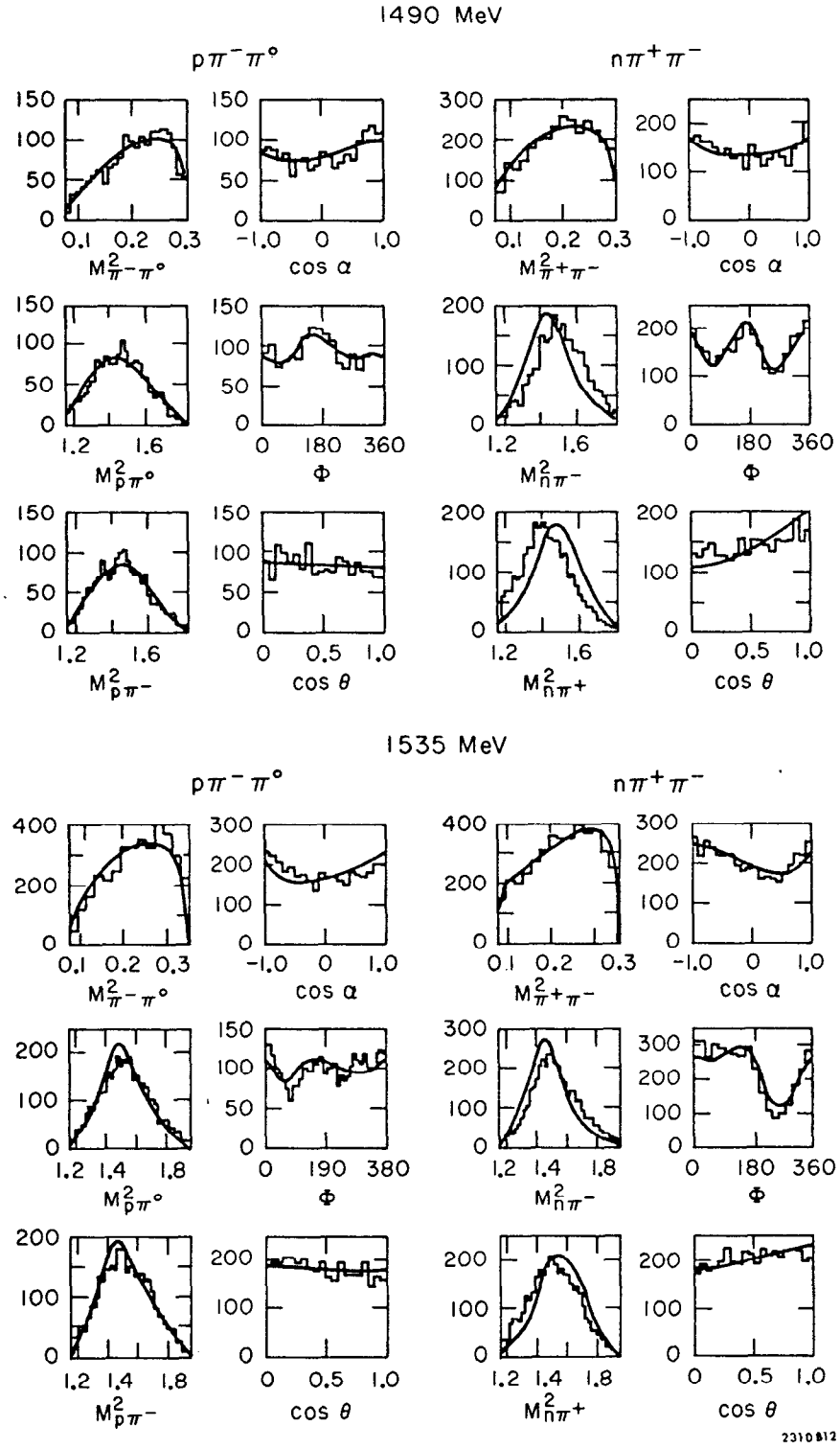

FIG. 7--Saclay fits to the data at c.m. energies of 1490 and 1535 MeV.

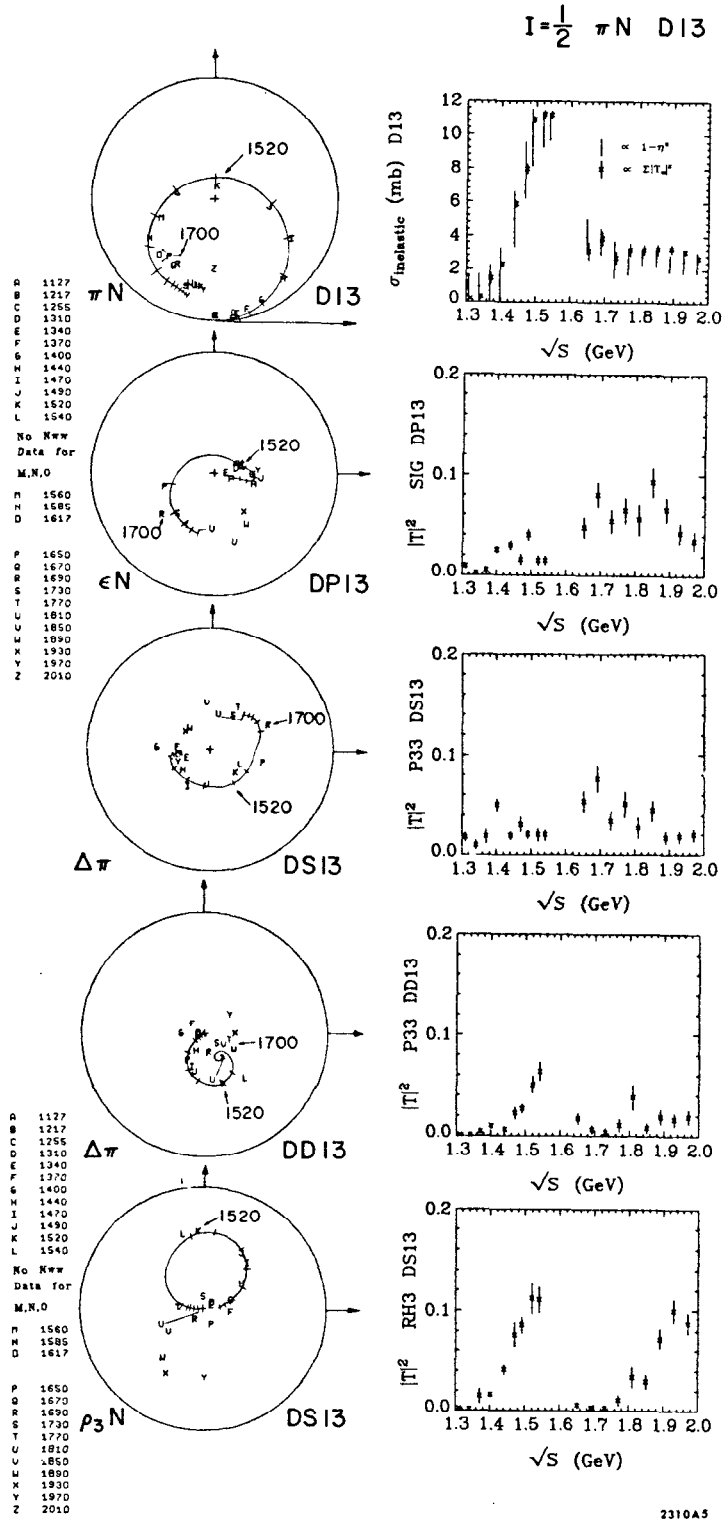

FIG. 8--Partial waves derived from the incident D13 wave.

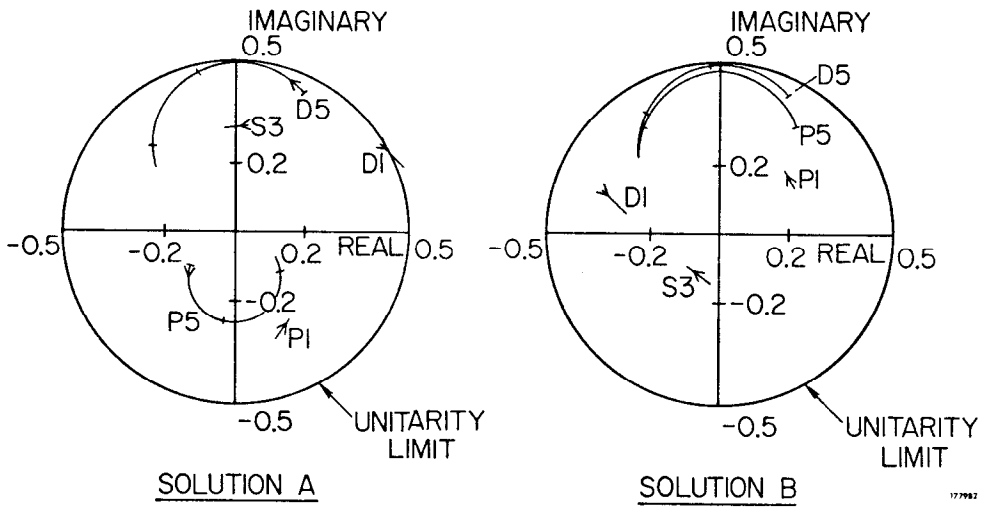

FIG. 9--D15 and F15 $\pi\Delta$ partial waves from the analysis of $\pi^- p \rightarrow \pi^+ \Delta^-$.

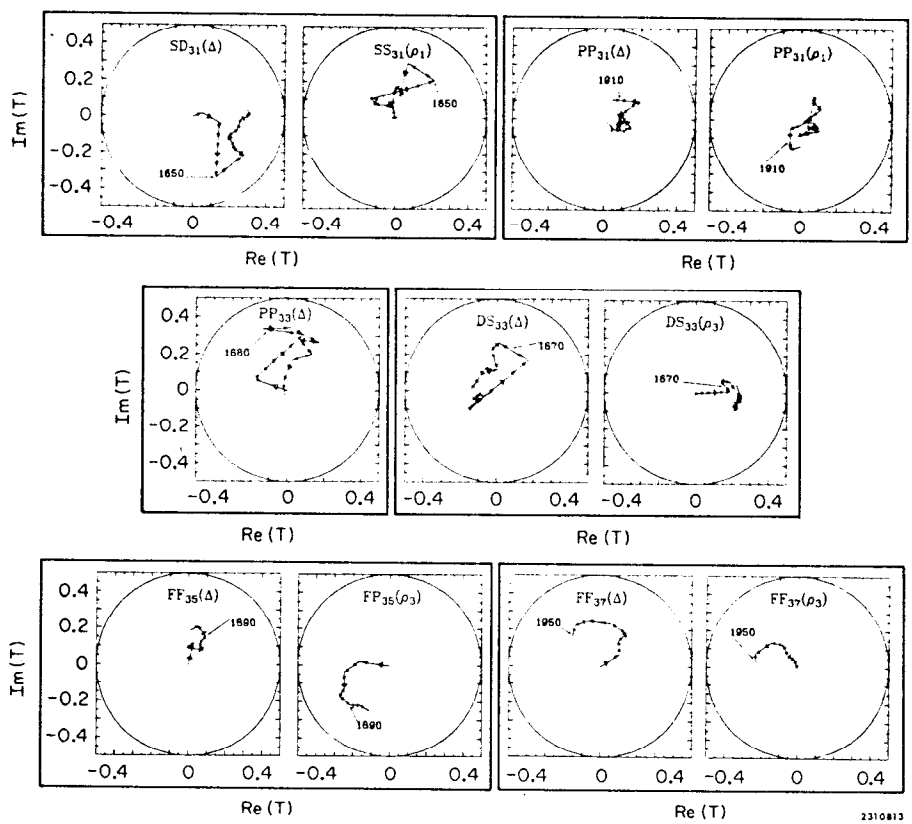

FIG. 10--I=3/2 partial wave amplitudes. Arrows are spaced every 20 MeV, with wide arrows every 100 MeV: base of wide arrows mark integral hundreds of MeV. Lower-ℓ waves are plotted starting at s=1400 MeV; higher-ℓ waves only where they were first needed. Last arrowhead is always at 1940 MeV.

1. For E < 1540 all I=3/2 amplitudes are small whereas at E $\geq$ 1650 (where we again have data) the S31, D33 and P33 waves are already large. This means that we are limited to observing only the high energy sides of the resonances in the S31 and D33 waves and are unable to see the complete anti clockwise motion in the Argand diagrams.

2. F35. As shown in Fig. 11 this resonance is observed in the f wave of the $\pi\Delta$ system although one might expect, on kinematical barrier factor

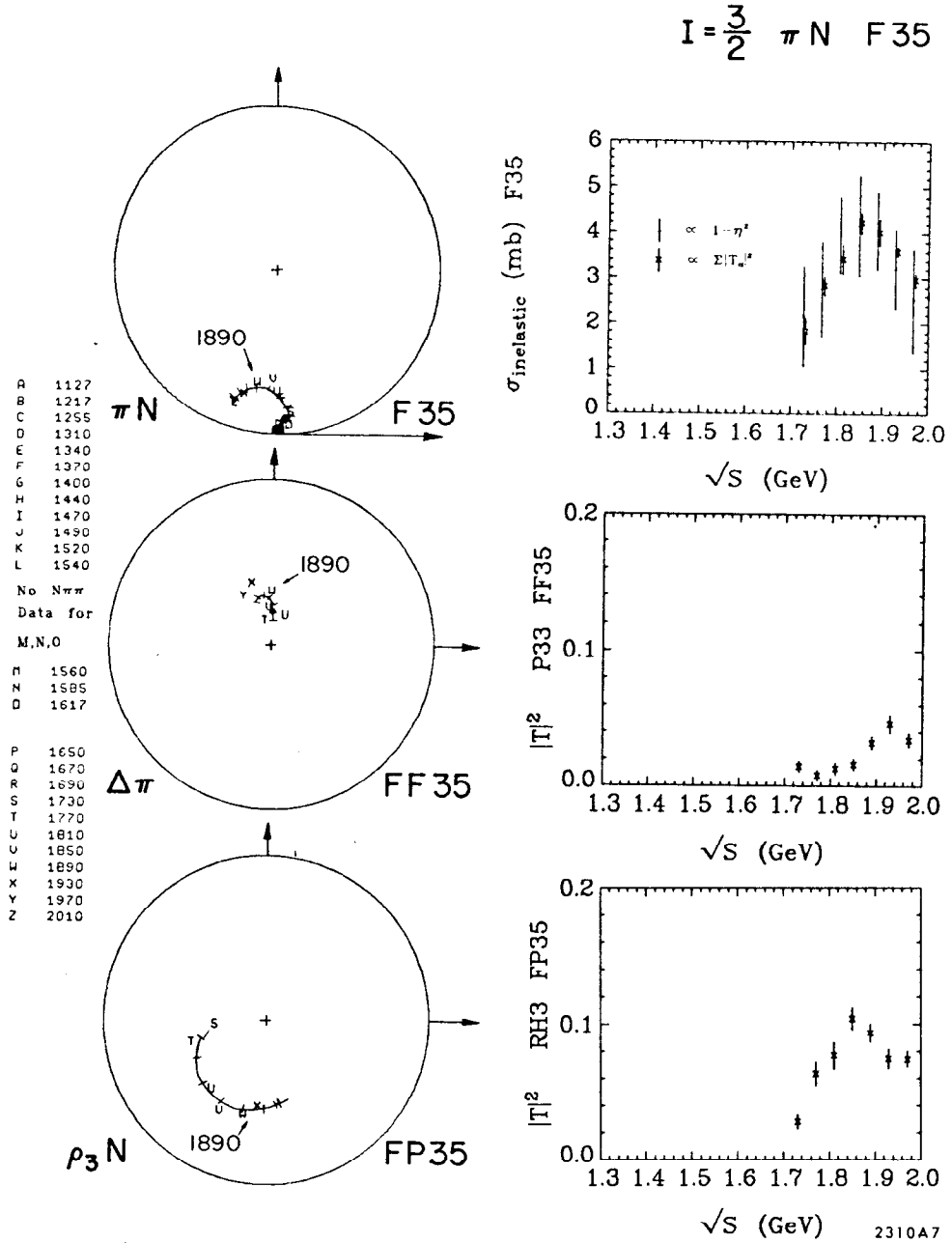

FIG. 11--Partial waves derived from the incident F35 wave.

arguments, the p-wave to dominate. The decay into $N\rho$ dominates and this final state allows us to saturate the EPSA inelastic cross section prediction.

3. F37. This resonance is observed both in $\pi\Delta$ and $N\rho$ channels but these two do not saturate the predicted inelastic cross section as demonstrated in Fig. 12. In fact, only ~60 - 70% is accounted for, a result

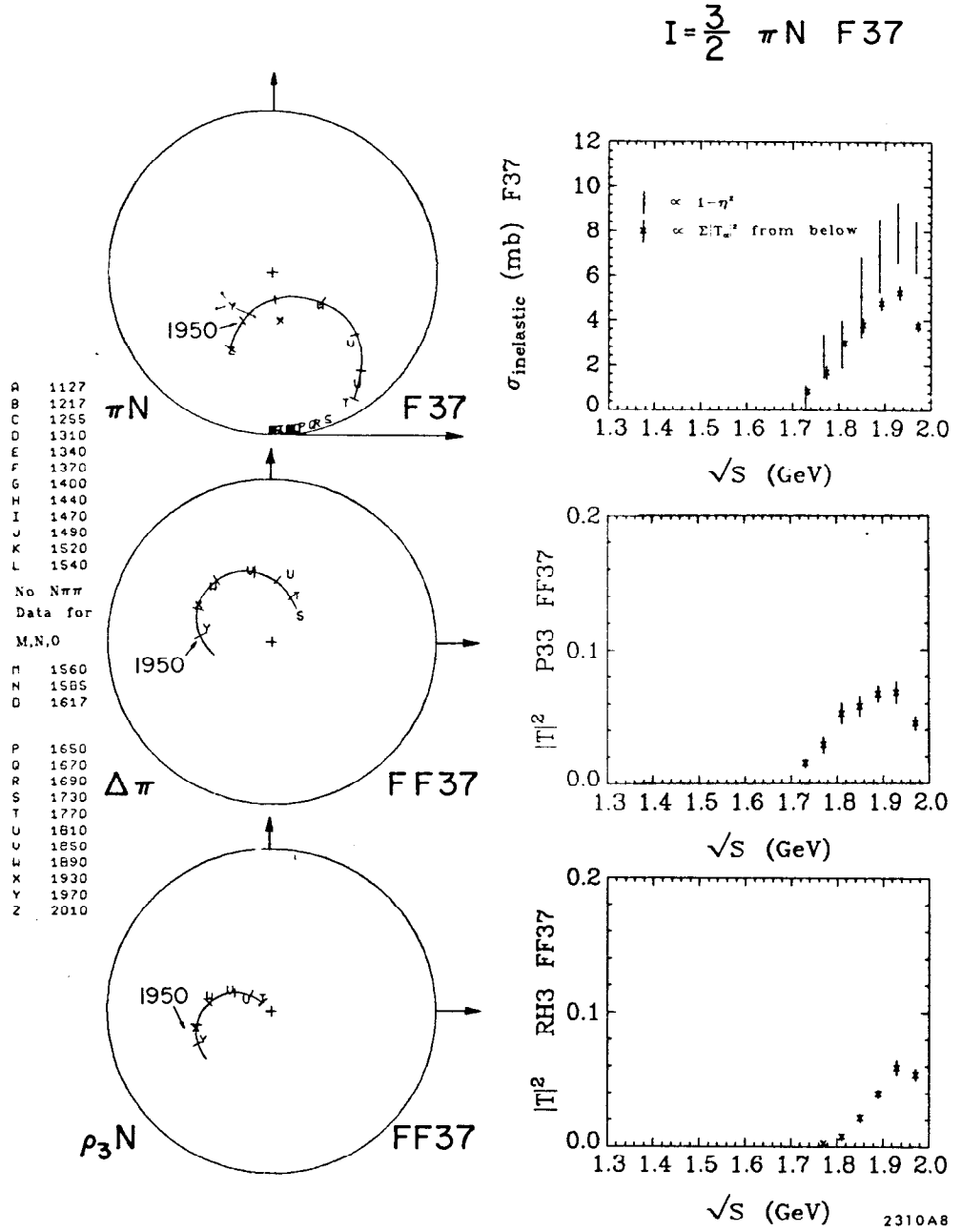

FIG. 12--Partial waves derived from the incident F37 wave.

which is consistent with the analysis of LBL/UCR.[12] The strong $N\rho$ coupling might well be expected again as this resonance is a dominant feature in photoproduction.

In general our results for the F35 and F37 resonance are qualitatively consistent with the analysis of LBL/UCR[12] in this energy region. Their $\pi\Delta$ f wave decays have the same relative sign as indicated in Fig. 13, an

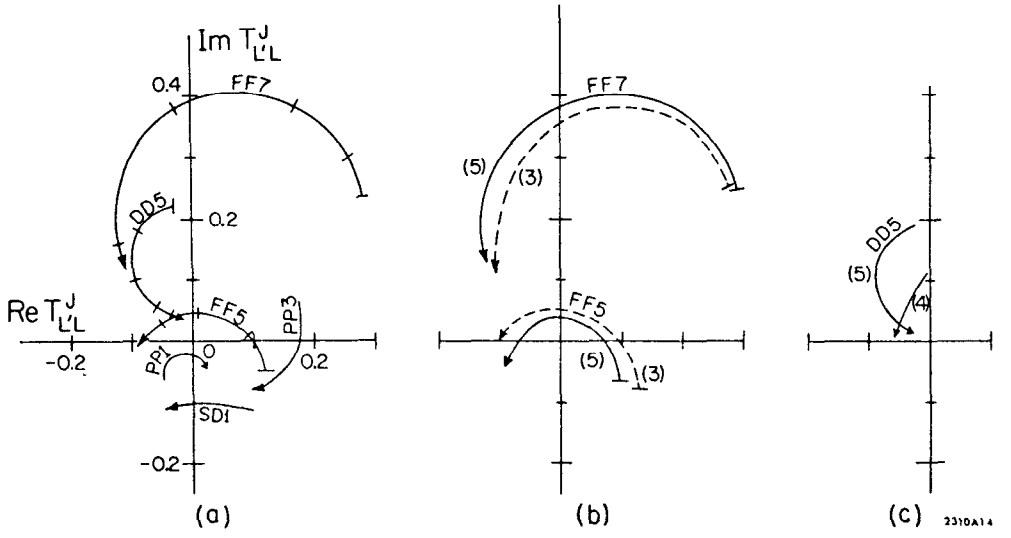

FIG. 13--F37 (FF7) and F35 (FF5) waves in the analysis of $\pi^+p \rightarrow \pi^0\Delta^{++}$ (a) gives the partial wave amplitudes in the best fit, (b) the variation in the F35 and F37 waves, and (c) the D35 wave.

Argand diagram of the partial waves in their energy dependent analysis. Their resonance couplings are larger than our observed values but their resonances are superimposed on comparatively large backgrounds. This results in the F37 resonance branching ratios being saturated ($\Sigma x_i \sim 1$) whereas they only account for ~70% of the inelastic cross section from the F37 wave. The dominance of the f-wave in the $\pi\Delta$ decays of these two resonances is consistent with predictions from duality.[18]

4. P33. From Fig. 14 it is clear that we have no indications of a P33 resonance for $E < 2000$ MeV, a state desperately needed in many classification schemes. Indeed the situation in this wave is very reminiscent of the behavior of the similar P wave[19] in

$$K^+p \rightarrow K^0\Delta^{++} \tag{12}$$

The presence of the two P_{11} states at low energies (~1470 and ~1750) imply the need for two P33 states in most schemes, while the [56, $L=2^+$] supermultiplet requires yet a third. There is evidence for one such state in EPSA at ~1900 MeV but there certainly is no such state in the region

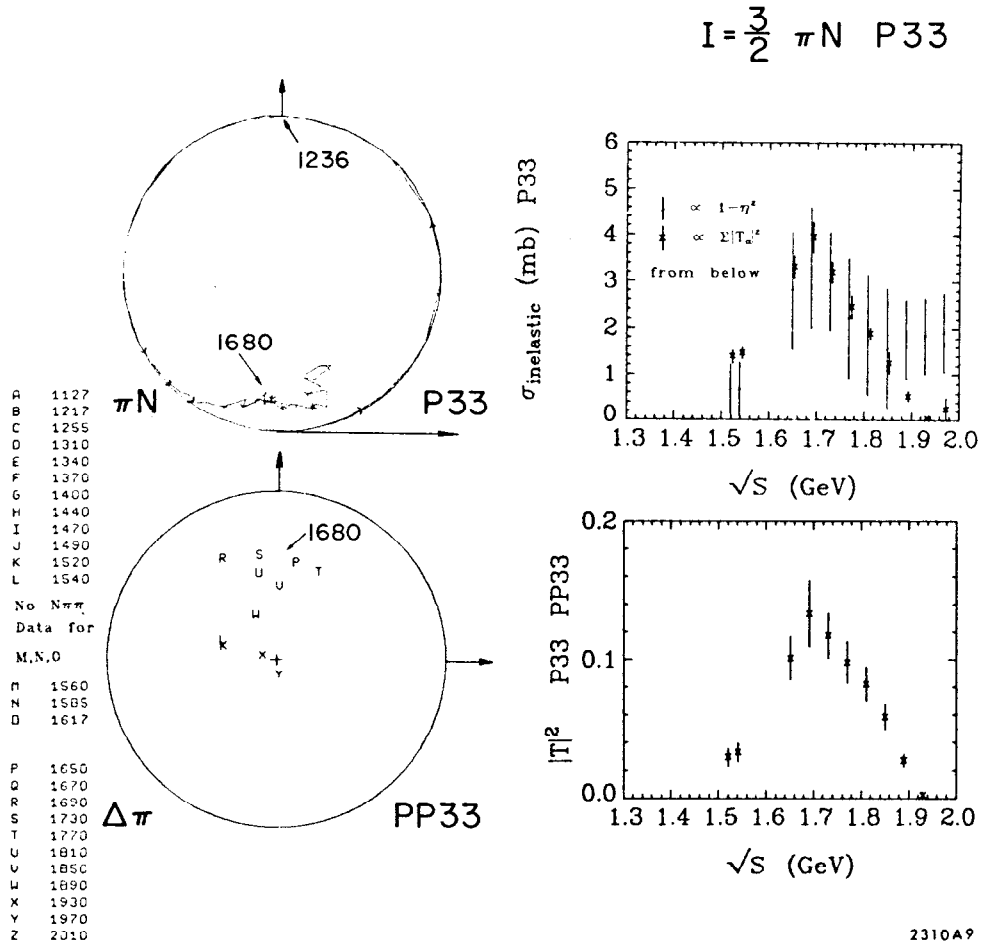

FIG. 14--Partial waves derived from the incident P33 wave.

of 1700 MeV. The absence of these states at low energies, unless they have remarkably small πN, $\pi\Delta$, etc., couplings or large mass splittings from their supermultiplet partners, must bring into question the present classification schemes.

5. P31, D35. For both of these waves we fall short of the EPSA prediction. In particular we find no need for waves derived from the incident D35 wave, i.e.,

$$\sigma(\mathrm{D35}) = 0 \quad .$$

Thus, if there are any low lying D35 resonances they do not couple to the $\pi\Delta$ or $N\rho$ channels. However EPSA does predict a large σ_{inel} from this wave (~4 mb) and this is a shortcoming of our results, although it probably has a natural interpretation as I will demonstrate in the following section.

C. Physics Not in the Analysis

In this section I want to draw some conclusions from our results of waves not being present or our failure to reach the EPSA prediction.

1. $\pi^+\pi^+n$ and $N^*_{\frac{1}{2}}$ final state interactions. Our predictions for $\sigma(\pi^+\pi^+n)$ are a factor of 2[2] too small (~ 2-3 mb unaccounted) at the higher energies. This is not surprising as only the $\pi\Delta$ intermediate states of our isobar model connect with this final state and from inspection of the π^+n mass spectra it is clear that $N^*_{\frac{1}{2}}$ intermediaries (P_{11}, D_{13}, F_{15}, D_{15}) may be present. Furthermore, [2] if one considers low angular momenta in the $\pi N^*_{\frac{1}{2}}$ system one finds:

$$\left.\begin{array}{ll} \pi\, D_{13} & \text{p-wave} \\ \pi\, F_{15} & \text{s-wave} \end{array}\right\} \quad \text{are derived from D35}$$

$$\pi\, P_{11} \ \text{s-wave} \quad \text{would be derived from P31}$$

which suggests that our, previously noted, failure to reach the P31 and D35 predictions is associated with not including N^* final state interactions. This suggestion can be further substantiated if we note that

$$\sigma_{\text{missing}}(\text{P31} + \text{D35} + \text{F37}) \simeq \sigma_{\text{missing}}(\pi^+\pi^+n) + \sigma(\pi\pi\pi N)$$

Finally the inclusion of these waves would have an appreciable effect in the $\pi^+\pi^+n$ final state whereas Clebsch-Gordon coefficients reduce their effect in the other single pion production reactions (9) so that our analysis of those channels would probably show little change.

2. Peripheral nucleon. The deterioration of the fits at higher energies is generally associated with being unable to entirely account for the onset of peripheral processes. This probably indicates the necessity for inclusion of π-exchange in the production of the $N\rho$ final state, so that higher partial waves are generated.

3. Limits for the observation of partial waves. In our analysis we estimate that any inelastic partial wave for which

$$|T| \gtrsim .06 \text{ to } .09$$

would be observed. If we consider this limit applied to a resonant amplitude this means that an unobserved resonance must have

$$\sqrt{X_{el}X} < .09$$

or

$$X_{el}X \lesssim 10^{-2} \quad .$$

V. QUANTITIES OF INTEREST FROM PARTIAL WAVE ANALYSES

In this brief section I wish to extract the quantities from these Argand diagrams that are valuable for theoretical tests but do not require terribly sophisticated analysis.

A. Coupling Signs

In this partial wave analysis we have measured 23 relative coupling signs and these are summarized in Fig. 15. These have been estimated from the Argand diagrams and are consistent with the results of the more sophisticated multichannel analyses I will describe later. Only the F37 $N\rho$ coupling is not consistent with an "eyeball" extraction and this is due to a large repulsive background in the $N\rho \to N\rho$ channel causing essentially a 90° backward rotation.[20] When reliable results are available for

$$\Lambda^*, \Sigma^* \to \pi\Sigma^*(1385) \ ,$$

$$\to N\,K^*(1890) \ ,$$

$$\to \Lambda, \Sigma\rho$$

SU(3) comparisons can be made. At present the results on these reactions are not entirely satisfactory.[21]

However, within higher symmetry schemes the decays we observe may be related to πN, etc., decays. These signs are then a critical test of any such higher symmetry as Dr. Gilman will show.[22]

B. Coupling Strengths

The estimation of such numbers is fraught with pitfalls and it is difficult to give reliable results. In Table III I have summarized our measurements but some words of explanation and the prescription used in deriving the results are necessary.

Prescription: (1) $T_{res} \simeq \sqrt{X_{el}X_{inel}}$ is estimated from the Argand diagram by eye taking into as much account as possible the backgrounds which may be present. The c.m. energy E is the approximate energy at which this estimation has been performed.

(2) I use the values of Γ_{tot} and X_{el} from Ref. 2 in order to calculate Γ_{inel} and X_{inel}.

The numbers appearing in Table III in each inelastic channel are $\sqrt{X_{el}X_{inel}}$ and Γ_{inel}, and the final column corresponds to the sum of the branching fractions for the given resonance. I have also included the description of the partial wave. It should be noted that the X_{inel} are very sensitive to variation in X_{el} — the elastic branching fraction.

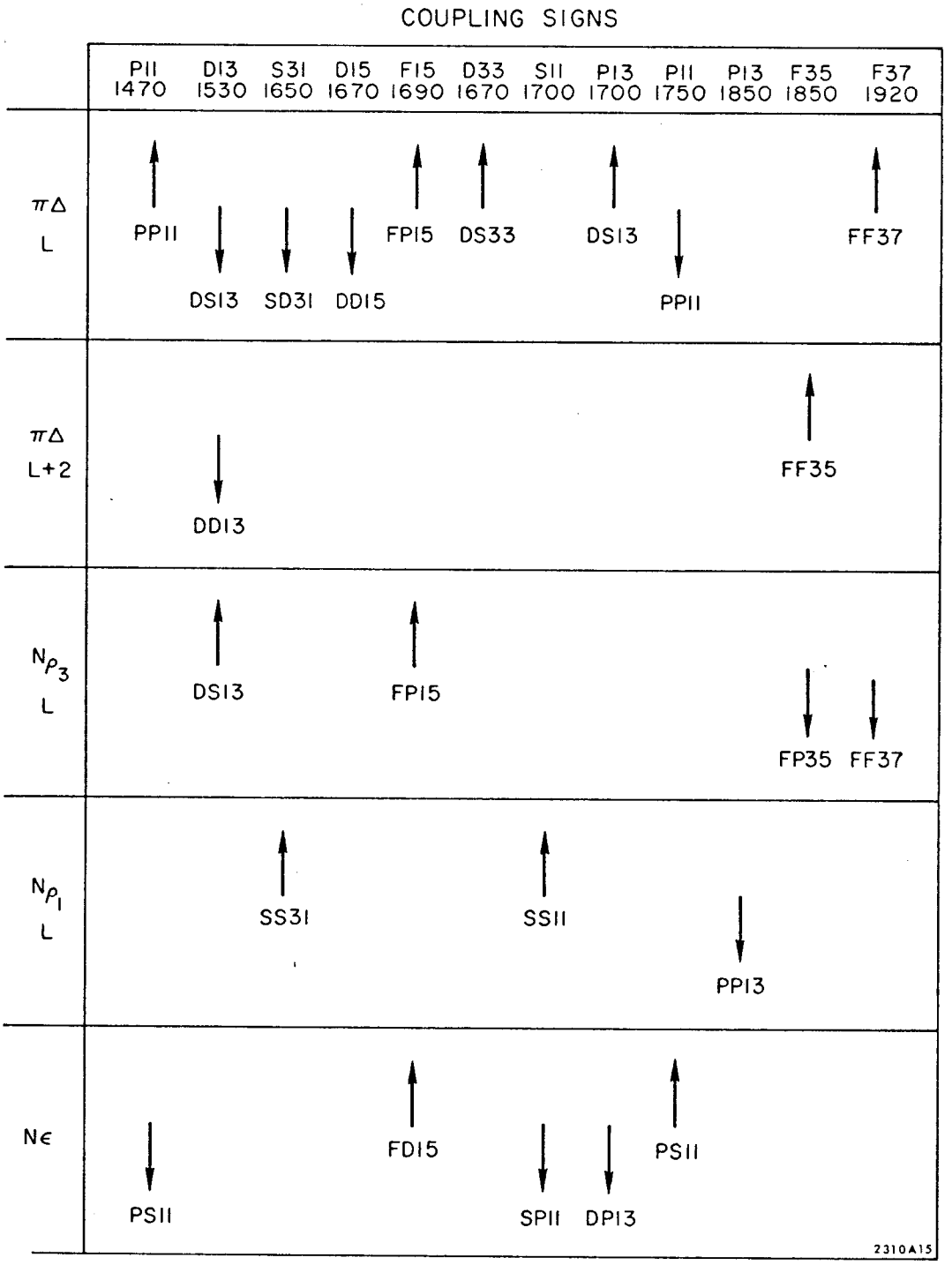

FIG. 15--Relative coupling signs of the resonances in all inelastic channels.

TABLE III

Summary of resonance couplings. Each entry contains the partial wave considered, the amplitude at resonance and the partial width in MeV.

Resonance	E (MeV)	Γ_{tot} (MeV)	x_{el}	$\pi\Delta$	$\pi\Delta$	$N\rho_3$	$N\rho_1$	$N\epsilon$	Σx_i
P11	1440	236	.52 124	PP11 +.29 36				PS11 -.25 28	.80
D13	1520	119	.57 68	DS13 -.27 15	DD13 -.21 9.0	DS13 +.31 20.0			.94
S31	1630	160	.32 51	SD31 -.325 52			SS31 +.307 47		.95
D15	1670	141	.40 56	DD15 -.46 75					.93
F15	1690	133	0.6 80	FP15 +.31 21		FP15 +.27 16		FD15 +.24 13	.97
D33	1670	207	0.16	DS33 +.37 172					.99
S11	1700	148	0.50 74				SS11 +.19 11	SP11 -.35 35	.81
D13	1730	130	0.10 13	DS13 +.11 17				DP13 -.29 109	1.07
P11	1750	183	.15 28	PP11 -.345 140				PS11 +.21 52	1.21
P13	1850	250	.25 63				PP13 -.44 195		1.03
F35	1890	260	.15 40		FF35 +.10 16	FP35 -.29 140			.75
F37	1930	230	.40 92	FF37 +.25 36		FF37 -.25 36			.71

Finally, one might note that in many cases all decay modes of the resonance are essentially accounted for ($\Sigma X_i \sim 1$).

C. Masses and Widths

In order to say anything sensible about these quantities one needs a reasonably accurate representation of the Argand diagrams. Qualitative estimates can vary by such large amounts[14] to make the results essentially useless. Descriptions of the Argand diagrams should be the final result of any multichannel fit to the data and thus I postpone comments on masses and widths until the next sections.

VI. MULTICHANNEL K-MATRIX AND T-MATRIX FITS

Our ability to account for all of the πN inelasticity in many partial waves indicates that we are now in the position to perform multichannel fits, exploiting the constraints of unitarity to their fullest possible extent, in attempting to understand the πN interaction. I want to further emphasize the point from my introduction that there will never be any essentially different information available from πN scattering — we have accounted for everything. We must now attempt the complete description of all the reactions occurring.

We have performed two types of multichannel analyses using

(i) the K-matrix formalism[23]

(ii) Breit-Wigner and backgrounds but made unitarity in all channels.[24]

We have concentrated on (i) because computationally it is simpler and so I will present results derived from it and then supplement these with a short discussion of (ii).

A. K-Matrix Fits and the Associated T-Matrix Properties

1. K-matrix parameters. If one fits the Argand diagrams we have determined within a conventional multichannel K-matrix[23] framework one immediately finds that many of the parameters, e.g., mass or couplings, have "ridiculous" values, e.g., if interpreted literally they correspond to resonance widths ~500 MeV where one can see from inspection of Argand diagrams that this is not the case. This is due, I believe, to the fact that one is not necessarily using the correct parameterizations for resonances and backgrounds. However one does obtain "good" representation of the Argand diagrams by this method.

2. T-matrix properties. If we have good representation of the Argand diagrams this implies that we have a comparatively good description of the T-matrix as a function of energy with our K-matrix formalism. In order to identify resonances and their properties we now search the T-matrix

for poles in the complex energy plane and determine the residues at these poles. The motivations for this procedure are

(i) we expect the pole position and residues in the T-matrix to be unique irrespective of our parameterization of the T-matrix, providing, of course, that it is good. This expectation stems from the work on the P33(1238) resonance[25,26] and investigations of our own.[27]

(ii) we expect the pole and residue to be closely related to the Breit-Wigner parameters but pole position does not equal M_0, $\frac{1}{2}\Gamma_0$ on the real axis and the residues are not necessarily equivalent to the widths.

We expect these equalities to become very poor when we either have large backgrounds or wide resonances.

The results of these investigations are contained in Table IV where I give the real and imaginary parts of the pole position together with the partial width calculated from the modulus of the residue at the pole. ($\Gamma = |\mathrm{Res}|^2 \times (\mathrm{Kin})$ where the kinematical factors are evaluated at $E=M_0$.) Several comments about these results are in order.

(i) Often the pole positions are a long way from the position one might expect, e.g., F35, F37, or P13.

(ii) $\frac{1}{2}\Sigma\Gamma_i \neq -\mathrm{Im}\, E_{pole}$ in many cases. This is not unexpected, the presence of background can easily produce such an effect. However, the main point to be made is that it is then not possible to go easily from pole residues to widths related to Breit-Wigners.

(iii) The last point is further emphasized by the fact that the residues have large phases even after taking into account the phases associated with kinematical factors.

The implication of these statements is that it is not easy (and sometimes impossible) to relate pole parameters to the conventional parameters of the Breit-Wigners we normally discuss. This point will be demonstrated more adequately in the following sections. It does appear, however, that these pole parameters are unique and thus it will be necessary for any future theories to present the results on resonances in terms of the properties of the corresponding second sheet poles (or whichever sheet is appropriate in the specific multichannel problem).

B. Unitary (Breit-Wigner and Background)

In this case we use conventional Breit-Wigners together with linear backgrounds but ensure the combination is unitary by application of the methods of Goebel and McVoy.[24] At this time we only have results for the D15 and F35 resonances and these are given in Table V. The complexity of the problem increases with the number of channels and hence resonances like the F15 take longer to analyze. However, if we use this parameterization

TABLE IV

Pole parameters and $\Gamma_{partial}$ from pole residues.

Wave	Pole	$\Gamma_{\pi N}$	$\Gamma_{\pi\Delta_L}$	$\Gamma_{\pi\Delta_{L'}}$	$\Gamma_{N\rho_3}$	$\Gamma_{N\rho_1}$	$\Gamma_{N\epsilon}$	Other Channel	$\Gamma_{tot}=\Sigma\Gamma_i$
S11	1 $1498 - i\frac{66}{2}$	11				11	34	14 (ηN)	70
	2 $1648 - i\frac{103}{2}$	46				12	4	32 (ηN)	94
P11	1 $1383 - i\frac{200}{2}$	80	40				5		125
	2 $1724 - i\frac{290}{2}$	120	37				75		232
P13	1 $1728 - i\frac{159}{2}$	25				84			109
D13	1 $1515 - i\frac{143}{2}$	90	38	15	34		3		180
	2 $1646 - i\frac{114}{2}$	16	22	3	3		62		108
D15	$1666 - i\frac{159}{2}$	69	92						161
F15	$1672 - i\frac{155}{2}$	101	12		42		21		182
S31	$1605 - i\frac{59}{2}$	17	11			35			63
D33	$1650 - i\frac{150}{2}$	13	56		56				125
F35	$1824 - i\frac{282}{2}$	44		26	107				177
F37	$1866 - i\frac{255}{2}$	111	76		57			132 (junk)	380

TABLE V

Comparison of resonance parameters from (a) coupling estimate and elastic phase shift analysis; (b) poles of the T-matrix; and (c) unitary (BW + background) fit.

	M	Γ_{tot}	πN	$\pi\Delta$	$\pi\Delta$	$N\rho$	$N\sigma$	
D15	1670	141	56	75				Elastic/coupling estimate
	1666	159	69	92				T-matrix pole
	1692	176	71	105				Unitary (BW+background)
F35	1890	260	40	16		140		Elastic/coupling estimate
	1824	282	44	26		107		T-matrix pole
	1907	324	51	55		219		Unitary (BW+background)
D13	1520	119	68	15	9	20		Elastic/coupling estimate
	1515	143	90	38	15	34		T-matrix pole
F15	1690	133	80	21		16	13	Elastic/coupling estimate
	1672	155	101	12		42	21	T-matrix pole
P13	1850	250	63			195		Elastic/coupling estimate
	1728	159	25			84		T-matrix pole

for the partial wave amplitude and search for the pole in the complex energy plane we find results consistent with those from the K-matrix parameterization.[27] These Breit-Wigner parameters are the ones conventionally used in SU(3), etc. comparisons.

C. Results from the Different Analyses

In Table V I have compared the various parameters one obtains for the resonances by the different methods one might employ

(i) using results from elastic analyses[2] (Breit-Wigner and background fit to elastic Argand diagram) together with estimates of coupling strengths from the Argand diagram.

(ii) T-matrix pole quantities from the K-matrix parameterization.

(iii) Unitary (Breit-Wigner and background) refit to smooth Argand diagrams from the K-matrix parameterization.

I think the lessons of this table are clear:

(i) for clear narrower resonances, e.g., D13, F15, D15, one obtains reasonable qualitative agreement although quantitatively there are factors of 2 (or more) disagreements in partial widths.

(ii) for wide resonances, e.g., P13, F35, the displacement of M_0 from Re E_{pole} can be of the order of 100 MeV.

The above observations mean that one should be wary of using quoted resonance parameters without checking their origin and further the partial widths are only reliable to factors of ~ 2.

VII. CONCLUSIONS

The conclusions can be summarized in the following manner.

A. Partial Wave Analyses of $\pi N \rightarrow \pi\pi N$

(1) The isobar model is phenomenologically fairly satisfactory, giving good fits to the data, characterized by partial wave amplitudes which are continuous in energy and saturate the predictions from EPSA. Moreover, these results are substantiated by PWA of selected subsamples of the data (e.g., $\pi N \rightarrow \pi\Delta$).

(2) We have positive evidence for the existence of a D13 resonance around 1700 MeV, whereas the existence of a P33 at similar energies is very doubtful.

(3) We have measured 23 couplings in sign and magnitude and this will be an important testing ground for any new theories.

(4) In the future one would like to analyze data in the region $1540 < E < 1650$ to complete the picture, add the $I=\frac{1}{2}$ isobar intermediate final states, and possibly introduce π-exchange contributions.

(5) Experimental results on the $\pi^0\pi^0 n$ final state and the measurement of single pion production from polarized targets would be valuable tests of our partial wave amplitudes.

B. Multichannel Fits and T-Matrix Poles

(1) It is possible to obtain good representations of the Argand diagrams in all channels and then extract the pole structure of the T-matrix. We have essentially completed this for all resonances for $E < 1900$ MeV using all the available data.

(2) It is not possible in general to relate the pole parameters unambiguously to the parameters of Breit-Wigners. If these latter quantities are required, one has to consider the lengthier job of fitting with a unitary (Breit-Wigner and background) parameterization.

(3) The uniqueness of the pole parameters indicated in analyses of the elastic P33 amplitude seems to be present in the inelastic waves we have considered.

C. Theoretical Implications and Challenges

(1) To produce theories of the resonance region which predict the observed analytic structure of the partial wave amplitudes, e.g., the pole parameters.

(2) To cope with the absence of P33 states in the SU(6) supermultiplet schemes.

(3) To produce a theory which can accurately predict the signs of all couplings and magnitudes to within a factor of 2 or so.

ACKNOWLEDGEMENTS

I would like to thank R. Longacre for his efforts in obtaining the resonance pole parameters, A. H. Rosenfeld and D.W.G.S. Leith for many critical comments throughout the analysis, M. Kugler and F. Gilman for instructive conversations. It is a pleasure to thank D.W.G.S. Leith for his support and interest.

REFERENCES

1. S. Almahed and C. Lovelace, Nucl. Phys. B40, 157 (1972).
2. R. Ayed, P. Bareyre, Y. Lemoigne, contributed paper to the XVI International Conference on High Energy Physics, Batavia (1972).
3. B. Deler and G. Valladas, Nuovo Cimento 45A, 559 (1966).
4. R. J. Cashmore, D. J. Herndon, and P. Söding, LBL-543 (unpublished).
5. A. D. Brody and A. Kernan, Phys. Rev. 182, 1785 (1969).
6. M. G. Bowler and R. J. Cashmore, Nucl. Phys. B17, 331 (1970).
7. W. Chinowsky, J. H. Mulvey, and D. H. Saxon, Phys. Rev. D2, 1790 (1970).
8. M. DeBeer et al., Nucl. Phys. B12, 599 (1969);
   M. DeBeer et al., Nucl. Phys. B12, 617 (1969);
   N. T. Diem, P. Chavanon, B. Deler, J. Dolbeau, M. Neveu, G. Smadja, G. Valladas, contribution to this conference.
9. D. J. Herndon, R. Longacre, L. R. Miller, A. H. Rosenfeld, G. Smadja, P. Söding, R. J. Cashmore, D.W.G.S. Leith, LBL-1065/SLAC-PUB-1108 (1972).
10. K. M. Watson, Phys. Rev. 88, 1163 (1952).

11. A. D. Brody, R. J. Cashmore, A. Kernan, D.W.G.S. Leith, B. G. Levi, B. C. Shen, D. J. Herndon, L. R. Price, A. H. Rosenfeld, P. Söding, Phys. Letters 34B, 665 (1971).
12. V. Mehtani, S. Y. Fung, A. Kernan, T. L. Schalk, Y. Williamson, R. W. Birge, G. E. Kalmus and W. Michael, Phys. Rev. Letters 29, 1634 (1972);
A. Kernan et al., contributed paper to this conference.
13. L. R. Miller, Ph.D. Thesis, LBL-38 (unpublished).
14. Particle Data Group, Phys. Letters 39B, 1 (1972).
15. P. Granet, P. Marly, P. Bareyre, P. Borgeaud, M. David, M. Ernivein, J. Feltesse, Y. Lemoigne, G. Villet, Amsterdam International Conference on Elementary Particles.
16. N. T. Diem, Thesis (Note CEA N-1602) Paris (1972).
17. R. Dalitz in Pion-Nucleon Scattering, eds. Shaw and Wang (John Wiley and Sons, Inc., New York, 1969);
O. Greenberg, Proc. Lund Conf., 1969, p. 398;
R. Feynman et al., Phys. Rev. D2, 1267 (1970).
18. Y. Gell, D. Horn, M. Jacob, J. Weyers, Nucl. Phys. B33, 379 (1971).
19. R. G. Bland et al., Nucl. Phys. B13, 595 (1969).
20. P. Coulter, Phys. Rev. 29D, 450 (1972).
21. C. Bricman, Invited talk at this conference on $K^-p \rightarrow \pi\Sigma(1385)$.
22. F. Gilman, Invited talk at this conference;
F. Gilman, M. Kugler and S. Meshkov, SLAC-PUB-1235 (1973).
23. R. D. Dalitz, Strange Particles and Strong Interactions (Oxford University Press, 1962).
24. C. J. Goebel and K. W. McVoy, Phys. Rev. 164, 1932 (1967).
25. T. Lasinski, L. Barbaro-Galtieri, Phys. Letters 39B, 1 (1972).
26. J. S. Ball, R. R. Campbell, P. S. Lee and G. L. Shaw, Phys. Rev. Letters 28, 1143 (1972).
27. R. Longacre, Ph.D. Thesis, LBL-948 (unpublished).